RSC Advances

ROYAL SOCIETY OF CHEMISTRY

www.rsc.org/advances

Graphical Abstract

Graphical Abstract for the article "**Chlorinated polyethylene (CPE)/ethylene methacrylate copolymer (EMA)/Sepiolite nanocomposite via a facile one-step covalent modification technique**"

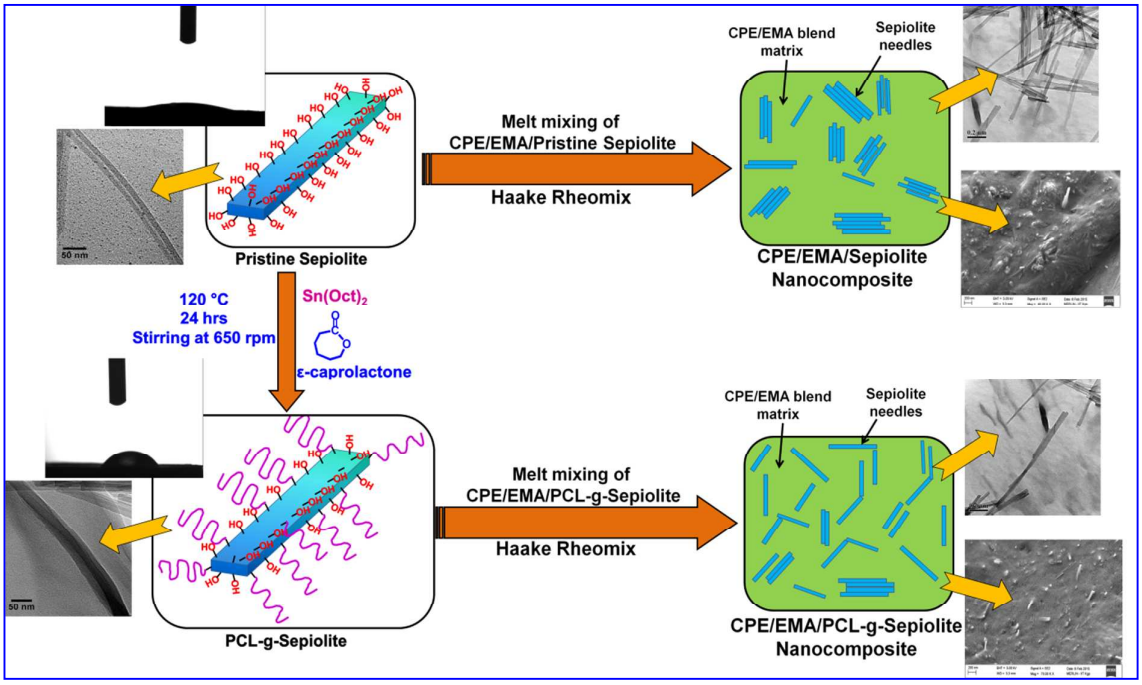

TOC

Facile one-step organo-modification of sepiolite improves polymer-filler interfacial adhesion, thereby advances mechanical property and thermal stability of CPE/EMA/sepiolite nanocomposite.

Chlorinated polyethylene (CPE)/ethylene methacrylate copolymer (EMA)/Sepiolite nanocomposite via a facile one-step covalent modification technique

Purabi Bhagabati, Tapan K. Chaki[*]*, Dipak Khastgir*

Rubber Technology Centre, Indian Institute of Technology Kharagpur
Kharagpur 721302, West Bengal, India
Correspondence to: Tapan K. Chaki (E - mail: tapanchaki2009@gmail.com)
Telephone number: +91-9434998508
Fax: 03222-282292

ABSTRACT

The work reports a facile one step covalent modification technique of sepiolite needles by *in-situ* polymerization of ε-caprolactone. The effective modification of sepiolite was confirmed by Fourier transform infrared (FTIR), X-Ray Diffraction (XRD), High Resolution-Transmission Electron Microscopy (HR-TEM) and water contact angle measurement. Nanocomposites of chlorinated polyethylene (CPE)/ethylene methacrylate copolymer (EMA) blend (60/40 ratio) were prepared by melt mixing the polymer blend with the pristine and poly(ε-caprolactone) modified sepiolite (PCL-g-SP). For the ease of comparison, equal filler content in both the nanocomposites was maintained (5 wt%). The effect of modified sepiolite on the mechanical and thermal properties of CPE/EMA blend of 60/40 ratio was precisely studied by ultimate tensile testing, dynamic mechanical analysis (DMA) and thermogravimetric analysis (TGA). The modified sepiolite based nanocomposite considerably showed a 47.77% improvement in ultimate tensile strength over the neat blend. Besides, a high char yield content of both the nanocomposites and 38.4% and 39.6% increment in the initial degradation temperature (T_i) values of pristine

and modified sepiolite based nanocomposites were observed respectively compared to the neat blend system.

KEYWORDS: Sepiolite, Nanocomposite, Mechanical property, Thermogravimetric analysis

1. INTRODUCTION

Chlorinated polyethylene (CPE) and ethylene methacrylate copolymer (EMA) are two commonly used saturated polymers in the field of cable, hose, pipe, and under the hood applications. The saturated ethylene backbone of the two polymer results high thermal stability, flame resistance property, chemical resistance, and excellent weatherability. Besides, CPE exhibits good mechanical properties. Blending CPE with EMA in various compositions results appreciable improvement in mechanical properties and thermal stability that is because of strong intermolecular force of attraction between the two polymers as reported by the same research group in earlier publication [1]. Development of polymer/inorganic nanofiller nanocomposites caused a remarkable improvement in mechanical, thermal, and physical properties compared either to the neat polymers or their conventional composites [2]. The key idea of polymer nanocomposites is grounded on its large interfaces, and high aspect ratio that undoubtedly causes reinforcement even at small loading (> 10 wt%) provided the condition of good polymer-filler interphase adhesion. One of the extensively employed inorganic nanofiller is montmorillonite (MMT), which is laminar smectite clay. Sepiolite is another type of clay that is known as reinforcing nanoparticle in various polymer matrixes and is currently receiving immense research interest [3-5]. Sepiolite is a natural fibrous clay mineral of ideal formula ($Si_{12}O_{30}Mg_8(OH)_4.(H_2O)_4 \cdot 8H_2O$) with hydrated magnesium silicate [6]. As like any other trioctahedral silicates, sepiolite also possesses ribbons of 2:1 phyllosilicate structures, where one ribbon is linked to an adjacent inverted SiO_4 tetrahedra [7]. The discontinuity of

the silica sheets in sepiolite gives rise to the characteristic structural tunnels and blocks of sepiolite along the fiber axis with a cross section [8]. These tunnels of sepiolite exhibit a sufficient quantity of H_2O molecules along with certain exchangeable cations such as Na^+, K^+, and Ca^{2+} [9, 10]. Unlike platelet-like clays such as MMT, the needle-like sepiolite is comparatively focused to the lesser extent in the literature. As reported by *Mittal et al*., the unique needle-like morphology offers an added advantage in terms of mechanical reinforcement over other clays [11]. Also, sepiolite needles proclaimed to display lower needle-to-needle contact area when it is compared to other layered phyllosilicates [12]. In addition to the needle-like morphology, the high surface area (BET 374±7 $m^2.g^{-1}$) of sepiolite, were demonstrated to act as a reinforcing nano-filler in some polymers [13-17]. As reported by *García-López et al*., an efficient organic modification of sepiolite is necessary that can drastically reduce filler-filler interaction and improve the polymer-filler interface adhesion [18, 19]. Because of the discontinuity of the external silica sheet of sepiolite, a significant number of silanol (Si–OH) groups are present on its surface [20]. The presence of such silanol groups at the edges of the tunnels increases the likelihood of effective organic modification of sepiolite. Reportedly, polymer nanocomposites with improved mechanical and thermal properties were been achieved by organic modification of sepiolite [21-23]. *Choudhury et al*. prepared HNBR-sepiolite nanocomposites and concluded that the interaction between sepiolite-polymer is the prime factor in improving mechanical properties of polymer nanocomposites [24]. *Fukushima et al*. reported to have improved polymer-filler compatibility and subsequently its dynamic mechanical properties by modifying sepiolite with poly(ε-caprolactone) and poly(lactic acid) [25]. Good polymer-filler compatibility is directly related to ameliorated dispersion of sepiolite in the polymer matrix that were studied by different methods [26]. *Frydrych et al*. also found greatly improved mechanical properties of gelatin/sepiolite nanocomposite foams [27]. *Duquesne et al*. reported the preparation of poly(ε-caprolactone)/sepiolite nanocomposites with improved mechanical, thermal, and morphological properties by following the two-step APTES-modified, PCL grafted sepiolite masterbatch [22]. However, single step direct covalent modification of sepiolite by PCL utilizing its surface silanol (Si-OH) groups as reactive sites for polymerization has not been reported till date. This work for the first time presents

a considerable improvement in the dispersion of sepiolite in CPE/EMA blend matrix by following a facile and one step method of organic covalent modification of sepiolite; and novelty of this work lies in here. Also, an attempt has been made to analyze the effect of better dispersion on mechanical, dynamic mechanical and thermal properties of CPE/EMA blend nanocomposite.

In this paper, ring opening polymerization of ε-caprolactone has been carried out in the presence of the sepiolite nanofillers. Here, the silanol groups (Si-OH) was used as site for the ring opening of ε-caprolactone and was pursued by chain growth polymerization. The modification of sepiolite was been characterized by Fourier Transform Infrared Spectroscopy (FTIR), X-Ray Diffraction (XRD), High Resolution-Transmission Electron Microscopy (HR-TEM) and contact angle measurement. Thenceforth, nanocomposites of CPE/EMA were prepared using the unmodified and modified sepiolite as masterbatches. A comparative study was performed on mechanical properties and thermal stability of pristine and PCL modified sepiolite based nanocomposites.

2. EXPERIMENTAL

2.1. Materials

Commercial grade CPE elastomer (CPE 360) with 36% Cl content, having density of 1.213 g cm^{-3} with Mooney viscosity $ML_{(1+4)}$ at 121 °C of 65±5 was obtained from East Corp International, India. Commercial grade of EMA, Elvaloy®1330 with 30% methyl acrylate (MA) content and a melt flow index (MFI) (at 190 °C/2.16 kg) of 3.0 g 10 min^{-1} (ASTM D1238) having melting point of 85 °C was obtained from NICCO Corporation, Shyamnagar, India. The monomer ε-caprolactone and catalyst Stannous octoate ($Sn(Oct)_2$) and Sepiolite (SP) powder were purchased from Sigma Aldrich, India. Magnesium oxide (MgO) of density 3.58 g cm^{-3} was used as acid scavenger for hydrochloric acid (HCl) produced during processing and molding. Dibutyltin dilaurate (DBTDL) and Irganox® 1010 which were procured from Sigma Aldrich were used as heat stabilizer of CPE and as antioxidant, respectively.

2.2. Methods

2.2.1. Covalent modification of Sepiolite

The sepiolite nanofiller was organically modified with poly(ε-caprolactone) (PCL) via. *in-situ* ring opening bulk polymerization of ε-caprolactone. In this technique, first the sepiolite needles were swollen by ε-caprolactone followed by ultrasonication for 30 mins in an inert atmosphere (N_2). A dry toluene solution (7 mL) of catalyst stannous octoate $Sn(Oct)_2$ was injected into the reaction chamber. Then the reaction was initiated by exposing the reaction mixture to 120 °C under nitrogen atmosphere. The reaction was stopped after 24 hrs by temperature quenching and then the resulting product was precipitated from cold methanol. It is named as PCL-g-SP and further it was recovered by filtration using THF. The obtained product was re-dispersed in THF by ultrasonication and then filtered again with fresh THF. The process was repeated at least for four times to ensure removal of any un-grafted/or loosely bound PCL polymers as similarly reported by Zeng *et al*. [28].

2.2.2. Preparation of C60E40 nanocomposites

CPE/EMA blend of 60/40 ratio was the base polymer matrix for the nanocomposites. First, CPE was melted at 140 °C for two minutes along with the additives MgO, DBTDL, and Irganox® 1010 that was followed by the addition of EMA and the mixing continued for another 4 minutes. Then the synthesized PCL-g-SP and pristine sepiolite of equal quantity were added into the internal mixer, and the mixing was continued for another 6 minutes. Sheets of 2 mm thickness of all mixes were prepared by compression molding. A concentration of 5 wt % inorganic content is targeted in each nanocomposite once the amount % grafting of modified sepiolite is determined. The nanocomposite of pristine sepiolite and PCL-g-SP is designated as C60E40/SP and C60E40/PCL-g-SP respectively. (*other ingredients are quantitatively equal in all samples (MgO, DBTDL, and Irganox® 1010 are in 3, 1, and 1 phr respectively) and compositions are in phr w.r.t. base polymer)

2.2.3. Characterization techniques

In order to confirm the successful synthesis of PCL and to inquire the presence of interaction between PCL with sepiolite Fourier transform infrared (FTIR) spectroscopy studies were performed. The FTIR spectroscopy studies were performed on a Bruker Equinox 55 spectrophotometer, at a resolution of 2 cm^{-1}, in the range of 4000–400 cm^{-1}, and 64 scans were averaged out for each spectrum. X-ray diffraction (XRD) study was carried out to examine the morphology of pristine and modified SP and their nanocomposite samples. The measurements were performed on Philips PW-1710 X-ray diffractometer (Eindhoven, The Netherlands), with crystal monochromated CuK_α radiation (λ=1.54 Å) in the angular range of 1–40° (2θ). The water contact angle of the unmodified and modified sepiolite was measured by a contact angle goniometer (Rame-Hart instrument Co., Model 190F2). Following the originally proposed procedure by *Rogers et al*., a pressure of 30 MPa was applied to the powder samples with a metal plunger for 5 s at room temperature in order to obtain 3 mm thick compact clay disks [29]. The prepared nanocomposites were cut into dumbbell-shaped test specimens (type V) according to ASTM D638-08 for analyzing the physico-mechanical properties. The testing was carried out in a Hioks–Hounsfield Universal Testing Machine (Test Equipment, Ltd., Surrey, England) at a cross-head speed of 500 mm min^{-1}, at room temperature. The bulk morphology of pristine and modified sepiolite was analyzed by high-resolution transmission electron microscopy (HRTEM) using a JEM 2100 JEOL transmission electron microscope with a lanthanum hexa-boride target, operating at 200 kV and with an average beam current of 116 μA. The solutions of both pristine and modified sepiolite were drop casted in carbon coated copper grid. The dispersion and distribution of HNT fillers in the polymer matrix were observed through HRTEM analysis of the ultramicrotomed samples. The surface morphology of prepared nanocomposites were analyzed by using field emission scanning electron microscopy (FE-SEM) ZEISS MERLIN GEMINI 2®, operating at 5 kV.

3. RESULTS AND DISCUSSION

3.1. Characterization of pristine and covalently PCL modified sepiolite

3.1.1. FTIR analysis

FTIR analysis of pristine and PCL modified sepiolite was done in order to find the type of chemical modification taking place on the surface of Sepiolite. In case of layered silicates, the hydroxyl groups are present mostly at the edge of the aluminosilicate platelets. Whereas, the silanol groups of sepioite are present over the whole external surface. This increase in number of free SiOH group is an outcome of the discontinuity in the octahedral sheets of Sepiolite, which cleaves Si-O-Si bond [30, 31]. Reports are available for the replacement of such free surface silanol groups of the inorganic clay surface with different organic modifier [32-34]. Organophilization of such highly hydrophilic clay fillers result in its enhanced compatibility with polymer matrix, which helps efficient interfacial stress transfer. Here, the covalent surface modification of sepiolite was carried out by following the *in-situ* ring opening polymerization of ε-caprolactone using stannous octoate as catalyst. First, the dried pristine sepiolite was homogenized with the ε-caprolactone monomer in the reactor by stirring. The reaction was activated by adding catalyst stannous octoate to the reaction mixer at 120 °C. Here, the free surface silanol groups of sepiolite act as initiator. The catalyst stannous octoate forms active complex sites with the hydroxyl groups of sepiolite as illustrated in Figure 1 (a) [32, 33].

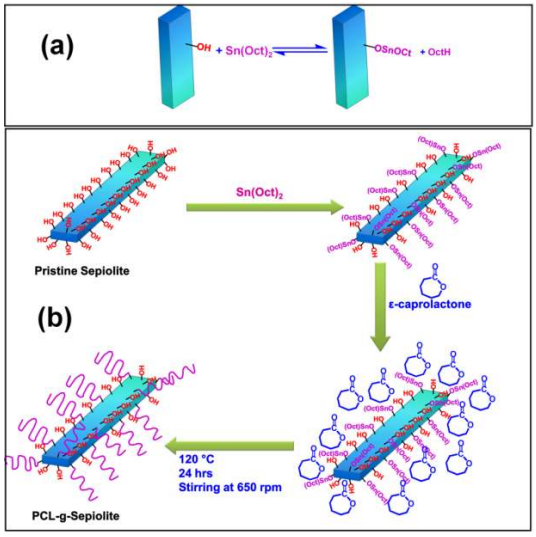

Figure 1: Schematic illustration of (a) formation of active sites for ring-opening polymerization on the sepiolite needle surface and (b) grafting of PCL chains onto the surface of sepiolite during *in-situ* polymerization

This complex that is attached to the sepiolite surface is responsible for initiating the ring opening polymerization of ε-caprolactone. The whole process is schematically represented in Figure 1 (b). In the reaction mixture during polymerization of ε-caprolactone, two types of PCL chains get formed; physically bound and covalently bound PCL. The physically bound PCL chains can be removed by repeated washing with solvent tetrahydrofuran (THF). Whereas, the PCL chains that are covalently grafted onto the sepiolite surface and cannot be removed simply by washing with THF. FTIR analysis was carried out for the pristine and PCL modified sepiolite and is shown in Figure 2. The characteristic bands of pristine sepiolite in Figure 2 are as follows: the O—H stretching vibration of structural water is at 3694 cm^{-1}; the bands at 3655 and 3564 cm^{-1} are ascribed to the Mg—OH groups [35]; a broad extended band for the zeolitic water at 3404 cm^{-1}; the $\delta_{H—O—H}$ of the coordinated bonded water is at 1665 cm^{-1} [36]; the $\nu_{Si—O}$ of Si—O—Si are at 1210, 1021-975 cm^{-1} (Si-O-Si in-plane vibration) [37]; the peak at 787 cm^{-1} is due to OH deformation vibration; and the bands at around 690 and 645 cm^{-1} are attributed to the Mg_3OH bending vibrations [38].

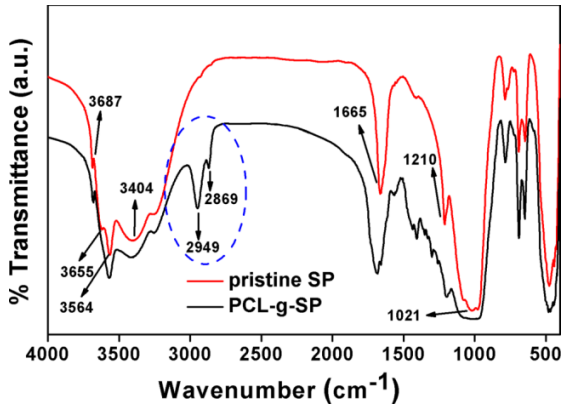

Figure 2: FTIR spectra of pristine and PCL modified sepiolite

The FTIR spectrum suggests that the surface pristine sepiolite contains sufficient quantity of bonded and zeolitic water, and –OH groups. The –OH groups available along the axis of sepiolite acts as the site for modification [18]. However, some new peaks were observed to be appeared in the modified sepiolite as indicated with the blue color circle. The new characteristic bands at 2949 and 2869 cm^{-1} are assigned to ν_{as} and ν_s of C—H bond of —CH_2— group of PCL chains. Moreover, the broadness of the peak at 1683 cm^{-1} and 1659 cm^{-1} is due to overlapping of the carbonyl (C=O) stretching vibration with the sharp peak of

$\delta_{H—O—H}$ [39]. Besides, the area of the bands between 3000 and 3800 cm^{-1} decreased after modification of sepiolite [40]. The above mentioned spectra of PCL modified sepiolite indicates that effective ring opening polymerization of ε-caprolactone at the surface of sepiolite took place.

3.1.2. Contact angle measurement

Contact angle measurement is one of the conventional techniques to measure the hydrophobicity of organo-modified inorganic fillers. The higher contact angle value means better hydrophobicity which in turn directly reflects the high degree of grafting. A goniometer was used to measure the contact angles of the water on pristine and modified sepiolite as shown in Figure 3.

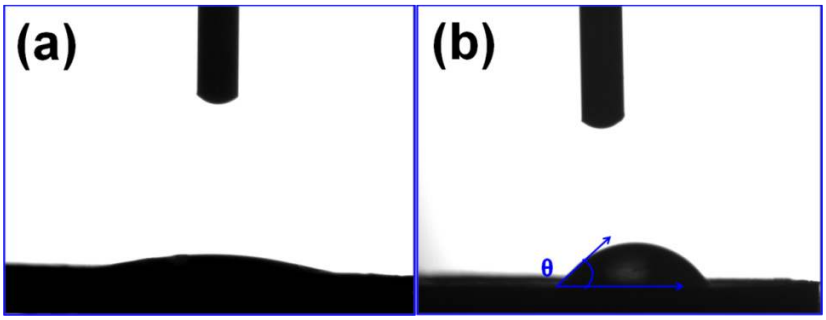

Figure 3: Contact angles of (a) Pristine sepiolite and (b) PCL-g-SP

It is clear that when de-ionized water droplet (10 μL) was dropped onto the surface of pristine sepiolite, immediately the liquid spread apart in the powder. This suggests a strong hydrophilic character of pristine sepiolite (Figure 3 (a)). On the contrary, the PCL modified sepiolite showed an immense increase in the static contact angle value of θ = 53°. These results shown in Figure 3 fully corroborates with HRTEM and FTIR results as discussed in the preceding sections. Furthermore, the grafting efficiency of PCL on the surface of SP was assessed by TGA. The amount of PCL grafted onto the SP surface can quantitatively be determined by measuring the wt% of PCL in the solid clay-rich fraction. The organic PCL content in the so-produced PCL-g-SP was found to be 31.5 wt%. Hence, it can be claimed that *in-situ* ring opening polymerization of ε-caprolactone caused a greater degree of PCL chain grafting onto the sepiolite surface.

3.1.3. Morphology study using XRD and HR-TEM analysis

The XRD patterns of pristine and PCL modified sepiolite are presented within the range of 3° to 16° (2θ) in Figure 4. Three characteristic diffraction peaks were found in both the samples; d_{110} = 1.19 nm (2θ = 7.3°), d_{130} = 0.74 nm (2θ = 11.8°), and d_{040} = 0.66 nm (2θ = 13.2°) with no changes in peak position and d-spacing. This clearly indicates that functionalization takes place solely either by surface modification or partial replacement of zeolitic water of sepiolite [9, 13].

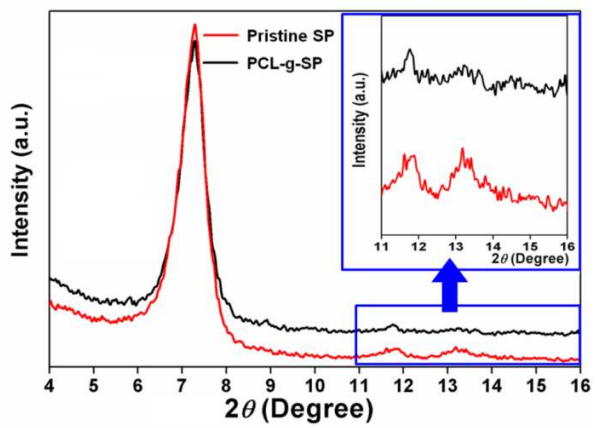

Figure 4: XRD patterns of pristine sepiolite and PCL-g-SP with magnified image within the range of 11-16° (2θ) inside the blue color box

Hence, the PCL modification caused no deformation of the crystalline structure of sepiolite. However, the intensity of all the three peaks got reduced in modified sepiolite. This reduced peak intensity of modified sepiolite demonstrates the grafting of a significant quantity of PCL chains on its surface. To confirm the modification of sepiolite from a structural point of view, HRTEM analysis were performed on both PCL-g-SP and pristine sepiolite for comparison. Representative HRTEM images and measurements of both samples are shown in Figure 5. The pristine sepiolite needle is noticeably straight with a uniform surface diameter of around 28 nm and longitudinally transparent at the middle. The high magnification TEM image of PCL modified sepiolite (Figure 5 (b)) evidently shows an uneven surface with increased outer diameter of around 49 nm.

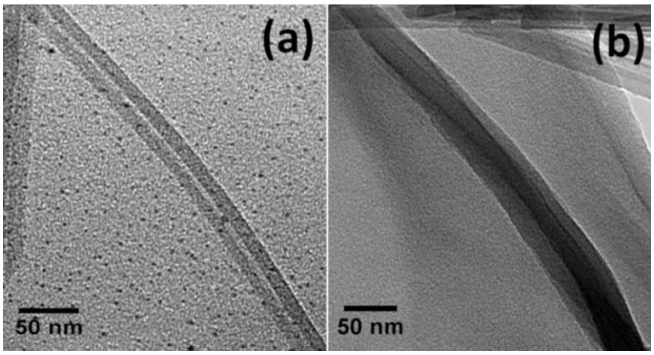

Figure 5: HRTEM images of (a) pristine sepiolite and (b) PCL modified sepiolite

A possible explanation for the PCL grafting on the surface of sepiolite depicted by HRTEM micrographs could be efficient ring opening polymerization of ε-caprolactone from the surface silanol groups at the edge of tunnels. The HRTEM results are in corroboration with the FTIR and contact angle data discussed in the preceding section.

3.2. Characterization of nanocomposites

3.2.1. Mechanical properties

Figure 6 (a), (b) and (c) shows the bar diagram of the ultimate tensile strength, % elongation at break values and tensile modulus at 100% elongation of unmodified and modified sepiolite nanocomposites respectively. The data of neat C60E40 is also taken into consideration for depicting better comparison. Emphasis has been put on the ultimate tensile properties by indicating the % improvement in tensile strength of the nanocomposites over the neat blend. As expected, the ultimate tensile strength of nanocomposites is found higher than the neat blend. This result supports the claimed reinforcing nature of sepiolite in polymer matrix in literature [23, 41, 42]. However, the pristine sepiolite based C60E40/SP nanocomposite suggests only a margin of 4.53% increment in tensile strength value over the neat blend. The most possible reason behind such minimal increment in tensile strength of C60E40/SP nanocomposite over the neat blend is the inadequate polymer-filler interfacial adhesion. The hydrophilicity of pristine sepiolite and hence the considerable polarity gap between filler and CPE/EMA blend matrix comes into

the picture. Nonetheless, the needle like structure and high aspect ratio of sepiolite reinforced the polymer matrix to a very little extent.

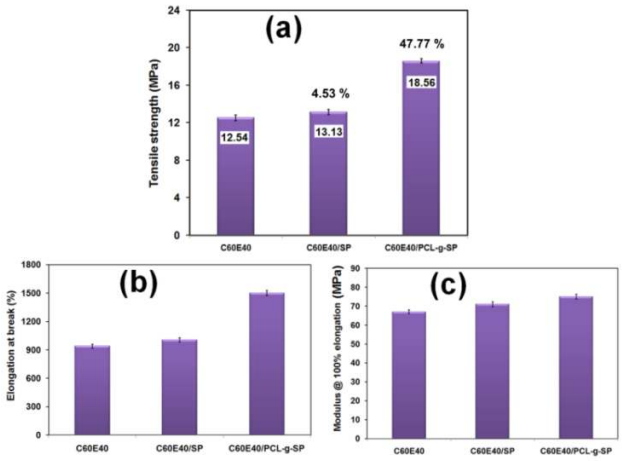

Figure 6: Column bar diagram of nanocomposites (a) Tensile strength, (b) Elongation at break, and (c) Modulus at 100% elongation of neat C60E40 blends and the prepared nanocomposites (an average value of 5 samples are taken)

On the other hand, the modified sepiolite based nanocomposite (i.e. C60E40/PCL-g-SP) showed enormous (47.77%) improvement in tensile strength value over the neat blend. This result can be explained on the basis of covalent modification of sepiolite by PCL that took part in developing filler compatibility with polymer. The organophilization of sepiolite by PCL (as evident from the contact angle data, FTIR and HRTEM analysis) increased polymer-filler interfacial interaction. Under severe mechanical shear during melt mixing, the good interfacial polymer-filler adhesion undoubtedly increased the state of filler dispersion. A uniform dispersion of fillers in nanocomposites is one of the deciding factors of its ultimate properties. The strong polymer-filler interactions with better state of dispersion of individual nano-sized sepiolite needles naturally influences the effectiveness of applied load transfer across the interfaces.

3.2.2. Micromechanical modeling

The ultimate tensile strength of a polymer composite is widely determined by strain hardening due to polymer chain orientation and polymer-filler interaction. According to

Interfacial adhesion reinforcing theory as mentioned by *Liang* [43], higher the polymer-filler interfacial adhesion, the better is the reinforcement of the polymer composites. Moreover, under the same interfacial adhesion strength, the larger the interfacial area of the fillers is positive for the reinforcement of the polymer composites. A semi-empirical equation on effect of spherical fillers in ultimate tensile properties of polymer composites was proposed by *Pukánszky* [44]. But recently, the model was successfully been applied to anisotropic fillers like sepiolite the needle-like nanoparticles, multiwalled carbon nanotubes (MWCNTs), wood fibers, and nano hydroxyapatite (nHA) nanorods [41, 45-47]. During tensile testing, the effective or true cross-section of samples incessantly reduces, resulting in higher value of true stress over the engineering stress. The effect of continual decrease in cross-section of the base polymer sample is independent of the presence of any second component. The true stress of polymers is the function of elongation and can be expressed as follows:

$$\sigma_T = \lambda \bullet \sigma \qquad \text{and} \qquad \lambda = \frac{L}{L_0} \tag{1}$$

Where, σ_T is the true stress, and σ is engineering stress of samples; whereas, λ is the relative elongations while the L_0 and L are the original and actual lengths of specimen. Under tensile mode, polymer chains undergo unidirectional orientation and the strength increases along the direction of oriented polymer chains. The increase in material strength due to the orientation of polymer chain along the direction of tension is called "*strain hardening*". The "*strain hardening*" effect can be expressed as:

$$\sigma_T = \lambda^n \tag{2}$$

The "n" is a parameter characterizing the strain hardening tendency of the base polymer matrix (in this case CPE/EMA blend) that can be calculated by a curve-fitting procedure. *Pukánszky* worked with various polymers, and the results of his work reflect that the strain hardening behavior of the polymer matrix is independent of filling [44]. It means regardless of the added fillers in the polymer matrix, the strain hardening behavior of the base matrix is

assumed to retain its characteristics. Hence, in this study the "n" value can be calculated from the slop of log-log plot of the true stress (σ_T) vs. the relative elongations (λ) of the unfilled CPE/EMA (60/40 ratio) blend.

In the absence of polymer-filler interfacial adhesion in a polymer composite system, the entire applied load is generally be carried by the polymer matrix. In that case, the decreased effective load-bearing capacity of the filled system has to be taken into consideration. In the present approximation, the minimum quantitative value of decrease in cross-section (A) of polymer matrix along the direction of applied load was taken into account by [48]:

$$A = \frac{1-\phi_f}{1+2.5\phi_f} \tag{3}$$

Where, ϕ_f is the filler volume fraction in the polymer matrix.

In polymer composites, when polymer adheres to the surface of fillers, the tensile strength increases. The expression adapted for tensile yield stress can also be adjusted for tensile strength:

$$\sigma_{Tred} = \sigma_{T0} \bullet \exp\left(B\phi_f\right) \tag{4}$$

Where, σ_{Tred} is reduced true tensile strength, σ_{T0} is the true tensile strength of polymer matrix and B is polymer-filler interfacial interaction parameter. The theoretical parameter B value primarily depends upon the interfacial strength between polymer and filler. Combining, Equation (2) – (4) gives the final expression:

$$\sigma_T = \sigma_{T0} \bullet \lambda^n \left[\frac{\left(1-\phi_f\right)}{\left(1+2.5\phi_f\right)}\right] \exp\left(B\phi_f\right) \tag{5}$$

$$B = \frac{1}{\phi_f} \bullet \log\left[\frac{1}{\lambda^n}\left(\frac{\sigma_T}{\sigma_{T0}}\right)\left(\frac{1+2.5\phi_f}{1-\phi_f}\right)\right] \tag{6}$$

Here, the "n" value of unfilled polymer matrix was determined from the plot of log σ_T vs. log λ as shown in Figure 7.

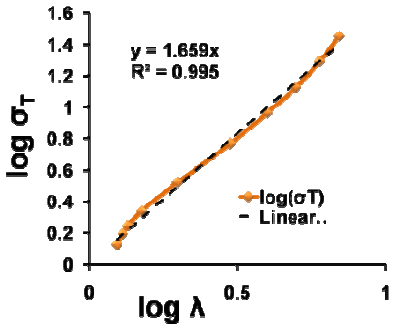

Figure 7: Strain hardening of unfilled polymer matrix (C60E40 blend) obtained from the slope of log σ_T vs. log λ plot

The "n" value in case of CPE/EMA polymer matrix is found to be 1.659 from the slope of the plot in Figure 7. B is an empirical parameter that can be determined for all the prepared nanocomposites by putting the experimental results in Equation (6). In this case, it is assumed that interfacial interaction is the only responsible factor for the observed differences in properties of the nanocomposites. As a basic line of thought, when polymer adheres to the filler, an interface gets created in between the polymer and filler. The property of this interface naturally dictates the overall mechanical properties of the composite. Good polymer-filler interfacial adhesion can potentially enhance the load-transfer efficiency in nanocomposites, which in turn causes higher B value. The model was earlier reported to be valid not only for individual polymer nanocomposites but also for polymer blend nanocomposites [49, 50]. The calculated B value obtained from the "*Pukánszky's model*" of Equation (6) for the C60E40/SP and C60E40/PCL-g-SP is found to be 1.13 and 3.06 respectively. It can be observed that the B value of modified sepiolite nanocomposites is higher than 2, which suggests good interfacial adhesion between the polymer matrix and PCL modified sepiolite. The B value lesser than 1 indicates weak interfacial adhesion; whereas, if B value is closer to 3, then the interfacial adhesion between polymer-filler will be strong enough to transfer the applied stress effectively [43, 47]. Hence, "*Pukánszky model*" supports understanding the relevance of polymer-filler interfacial

adhesion in the ultimate mechanical properties of nanocomposites. Moreover, the morphology of polymer nanocomposites has a tremendous effect on its mechanical properties that has to be taken into account for the study of its structure-property relationship. A comprehensive morphology study of the prepared nanocomposites has been made in the later section in order to understand its effect on observed mechanical properties.

3.2.3. Dynamic mechanical analysis (DMA)

DMA is widely accepted as one of the most helpful technique for evaluating the effect of filler addition in the polymer matrix. Figure 8 (a) and (b) displays the temperature dependency of tanδ and storage modulus (E') of neat polymer blend and its prepared nanocomposites over a temperature range of -75 °C to 100 °C, respectively. The temperature of the maximum of tanδ in the temperature sweep graph indicates the glass-rubber transition temperature (T_g) of the polymer matrix.

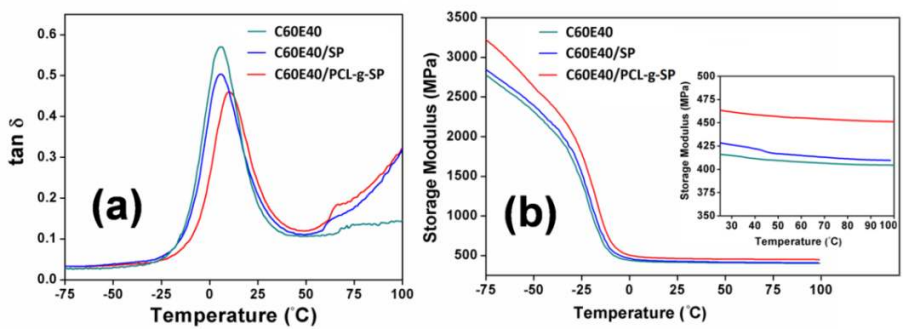

Figure 8: Temperature sweep of (a) tanδ and (b) storage modulus (E') of neat polymer blend and its (nano)composites

In filled polymer system, dynamic mechanical testing is often employed to study the effect of fillers on the T_g of polymers [51]. The pristine sepiolite nanocomposite (i.e. C60E40/SP) did not undergo any significant change in the T_g value from the neat C60E40 blend. This insignificant change in T_g indicates that the pristine sepiolite has little effect in reinforcing the base polymer matrix. The reason is that poor polymer-filler interfacial adhesion between pristine sepiolite and C60E40 blend matrix. The highly hydrophilic sepiolite surface barely

provides any scope for strong chemical or physical interaction with the polymer matrix. On the other hand, an appreciable shift in tanδ peak towards higher temperature is observed in the case of C60E40/PCL-g-SP nanocomposite. The successful and effective covalent grafting of organic PCL chains on the sepiolite surface (as evident from the FTIR analysis) improved polymer-filler interaction. The existence of strong polymer-filler interfacial interaction restricts a larger number of chains of the polymer matrix. The successful organophilization of hydrophilic sepiolite by PCL (evident from the water contact angle data and HRTEM analysis) also improved the state of filler dispersion during processing in the matrix. The damping (height of the tanδ peak) indicates the ability of the material for dissipating the applied energy and at T_g region the long range macromolecular chains attain mobility by dissipating energy through viscous movement [52].

Table 1: Glass transition temperature (T_g) and storage modulus (E') at -75 and 100 °C of all samples from DMA analysis

Sample designations	Glass transition temperature T_g (°C)*	Storage modulus E' at -75 °C (MPa)	Storage modulus E' at 100 °C (MPa)
C60E40	5.2	2720	100
C60E40/SP	5.8	2840	409
C60E40/PCL-g-SP	10.4	3229	455

* The glass transition temperatures for all samples are taken from the tanδ vs. temperature plot of DMA

Both the nanocomposites have undergone a clear broadening of tanδ peak over neat polymer matrix. Decreasing the height of tanδ peak means reduction of number of mobile macromolecular chains in its transition region. The improved interfacial adhesion between sepiolite and polymer matrix due to covalent grafting of sepiolite by PCL (PCL-g-SP) caused the formation of immobilized regions around the filler surface [53]. Moreover, the PCL polymer provides an added advantage of improved compatibility with CPE/EMA blend matrix. Figure 8 (b) shows the evolution of the storage modulus as a function of

temperature for C60E40 neat blend and its nanocomposites. The values of storage modulus below T_g (at -75 °C) and above T_g (at 100 °C) along with the T_g values are tabulated in Table 1. These curves indicate that the storage modulus of nanocomposites at low temperature (-75°C) below the T_g is clearly much higher than the neat polymer blend. It is worth to mention that the storage modulus below and above the glass transition temperature is primarily dictated by the strength of intermolecular forces existing between polymer-filler and the way polymer chains are packed [54]. The improved storage modulus of all (nano)composites over neat polymer is attributed to better polymer-filler interaction and improved dispersion of nano-sized sepiolite needles in the polymer matrix. The inset in Figure 8 (b) shows the behavior of variation of storage modulus at high temperature. It can be observed that the storage modulus above the glass transition temperature remains almost constant. Also, the E' value of C60E40/PCL-g-SP nanocomposite is showing the maximum value that is followed by C60E40/SP nanocomposite. Such behavior of storage modulus is naturally because of the reinforcing action of the sepiolite needles.

3.2.4. Thermogravimetric analysis (TGA)

The addition of clay nanofillers into polymer matrix has both positive and adverse effect on the thermal degradation stability of nanocomposites. Based on the chemical nature of polymer matrix, polymer-filler interaction, and the morphology of fillers inside the matrix; nanocomposites may show improved or inferior thermal stability over neat blend. A uniform dispersion of clay like nanofillers form nanocomposites that exhibit higher thermal degradation stability over any other high loading micro-composites [55, 56]. In order to investigate the effect of pristine and PCL modified sepiolite on the thermal stability of CPE/EMA blend nanocomposites, TGA study has been carried out in an inert atmosphere of N_2. The thermo-gravimetrograms and its derivatives of neat C60E40 blend and its (nano)composites are plotted in Figure 9 (a) and (b) respectively. Heating under inert gas flow causes non-oxidative degradation of materials. As can be seen from the Figure 9, the neat C60E40 blend and its nanocomposite decomposed with two-step weight loss.

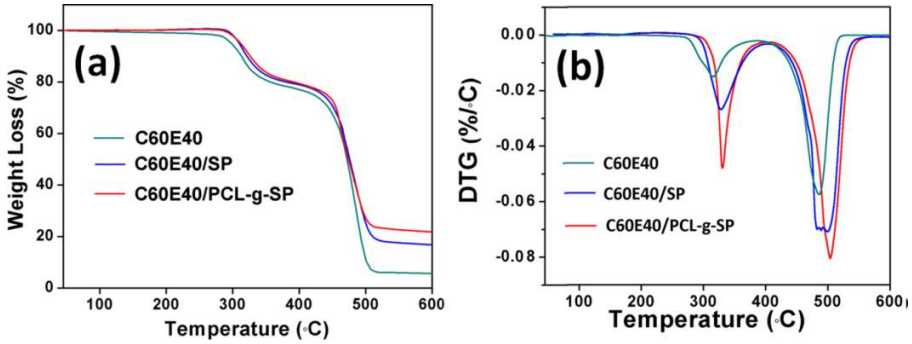

Figure 9: (a) TGA and (b) DTG plots of neat C60E40 blend and their (nano)composites

The first step is attributed to the evolution of hydrochloric acid (HCl) due to decomposition of CPE in the range of 250 °C to 370 °C. The second step in between the temperature range of 455 °C and 510 °C corresponds to the degradation of polyenes of CPE and EMA copolymer. From the TGA plot, the onset degradation temperature T_i, (corresponding to 5 wt% loss) and T_{50} (temperature corresponding to 50 wt% loss), the maximum weight loss temperatures of the mentioned two steps (T_{1max} and T_{2max}) along with their char yield (wt%) were tabulated in Table 2.

Table 2: TGA data of neat C60E40 blend and its prepared (nano)composites

Sample Designations	Initial degradation Temperature (T_i) (°C)*	Temperature at 50 wt% loss (T_{50}) (°C)*	Maximum weight loss Temperatures of Peak 1 (T_{1max}) (°C)	Maximum weight loss Temperatures of Peak 2 (T_{2max}) (°C)	Char yield content (wt%)
C60E40	212.0	471.2	314.5	485.3	5.13
C60E40/SP	293.5	473.7	327.8	498.7	16.67
C60E40/PCL-g-SP	295.2	475.1	330.7	503.9	19.19

* Ti is the temperature at 5% weight loss, and T50 is the temperature at 50% weight loss

The data in Table 2 reveals that the addition of sepiolite in both pristine and modified form into C60E40 matrix increased the overall thermal degradation stability significantly. The C60E40/SP and C60E40/PCL-g-SP nanocomposites showed an appreciable 38.4% and 39.6% increment in T_i values over neat blend. The incorporated sepiolite nanofillers into

the polymer matrix acted as a superior insulator, and mass transport barrier to the volatiles (like HCl) produced during decomposition [57]. The T_{50} values of both the nanocomposites are closer to each other and deviated about 5 °C from the neat blend. The increased T_{1max} and T_{2max} values of the nanocomposites and their higher char yield at 600 °C (Table 2) refers to the improved thermal stability of sepiolite nanocomposites. A significant increase in thermal degradation stability of sepiolite nanocomposite was reported in various literatures and was claimed to be because of good polymer-filler interaction [25, 58, 59]. The increased char yields of both the sepiolite nanocomposites (with equal filler wt %) can also be attributed to the entrapment of volatile HCL products inside the porous structure of sepiolite. Interestingly; the covalent modification of the sepiolite nanofillers by PCL further improved the thermal degradation stability of the nanocomposite. The improved thermal stability of clay nanocomposites is mainly the result of the formed char that hinders the diffusion of volatile products by creating a tortuous path known as "*Labyrinth effect*" [57, 60]. Sepiolite being needle like structure has less possibility for the tortuosity of the diffusion pathway in comparison to fully exfoliated platelet like nanoclay structures. But the improved thermal stability of PCL modified sepiolite nanocomposites by delayed diffusion of gasses is more likely related to extensive polymer-filler interaction. Such behavior has also been reported for sepiolite nanocomposites of PU, wheat starch and PE; and assigned to the strong polymer-filler interaction that is capable of forming a much thicker protective inorganic layer at the surface of the degrading material than montmorillonite [58, 61, 62]. Nanocomposites with a better state of filler dispersion generally lead to a higher thermal stability over the conventional micro-composites [63, 64]. The successful organic modification of sepiolite by PCL (as evident from the FTIR, HRTEM, and Contact angle data) organophilized the hydrophilic sepiolite and thereby reduce the filler-filler interaction. In this case, the grafted PCL chain plays a significant role in improving the polymer-filler interaction with CPE/EMA blend matrix. During melt mixing, good polymer-filler interface adhesion directly promotes the state of nanofiller dispersion in the nanocomposite under high mechanical shear. These parameters help the individual sepiolite needles to disperse homogeneously and randomly in nano level within the matrix. A better state of nanofiller dispersion in polymer matrix undoubtedly provides a positive impact on the thermal

degradation stability of nanocomposites. Hence, melt mixing of covalently modified PCL-g-SP with C60E40 blend is an effective way to develop nanocomposites with superior mechanical properties and improved thermal stability.

3.2.5. Morphology study of nanocomposites

Wide angle X-ray diffraction (WAXD) analysis

Morphology of prepared nanocomposites was studied using wide the angle X-ray diffraction analysis technique. It is one of the most frequently used techniques for examining the morphology of inorganic filler nanocomposite. WAXD study helps find the filler state of dispersion in the polymer matrix, which have an utmost importance in dictating mechanical and thermal properties of nanocomposites. The characteristic diffraction peak of (110) plane of pristine SP was found at $2\theta = 7.3$ ° with d-spacing of 1.1 nm in the inset of Figure 10. In the C60E40/SP nanocomposites, the peak for the (110) plane of sepiolite was observed at $2\theta = 7.1$ with a minor increase in d-spacing of 1.2 nm. Shifting of this peak is trivial and does not confirm any intercalation of polymer into the tunnels of sepiolite needles. Also, it can be anticipated from the intensity of the (110) plane of sepiolite that the dispersion of pristine sepiolite in the polymer matrix is weak. Such phenomenon is because of high filler-filler interaction between the hydrophobic sepiolite needles in the polymer matrix. However, the diffraction peak for (110) plane of sepiolite is vanished in C60E40/PCL-g-SP nanocomposites at the same level of filler concentration as for C60E40/SP. The disappearance of the characteristic (110) plane of sepiolite in the C60E40/PCL-g-SP apparently suggests an excellent state of sepiolite needle dispersion in the polymer matrix. Covalent grafting of PCL chains onto the surface of sepiolite improves polymer-filler interfacial interaction in the C60E40/PCL-g-SP nanocomposite.

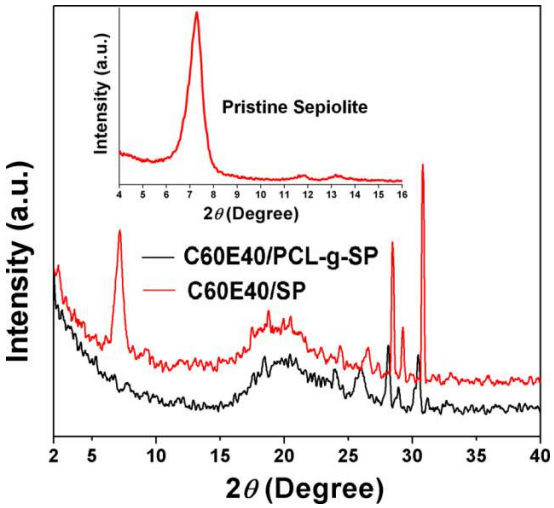

Figure 10: WAXD patterns of C60E40/SP and C60E40/PCL-g-SP nanocomposites

A precise characterization of PCL modified sepiolite by FTIR, HRTEM, and water contact angle measurement in the preceding section, distinctly demonstrates successful organophilization of sepiolite needles. During melt processing, under the influence of severe mechanical shear the PCL chains promoted compatibility of modified sepiolite with CPE and EMA matrix. Improved polymer-filler compatibility further increased the state of filler dispersion in the polymer matrix.

Transmission electron microscopy (TEM) analysis

The representative TEM analysis of the C60E40/SP and C60E40/PCL-g-SP nanocomposites was carried out in order to evaluate the quality of dispersion of sepiolite needles in the polymer matrix. The images in Figure 11 are provided at the same magnification of 0.2 μm for the ease of comparison. Images were taken from 10 different areas of the ultramicrotomed samples of each nanocomposite. The bright background shows the polymer matrix while the dark needle-like structures are individual sepiolite. The state of inorganic nanofiller dispersion in the polymer matrix is a powerful, decisive factor in determining the mechanical and thermal properties of nanocomposites [65, 66].

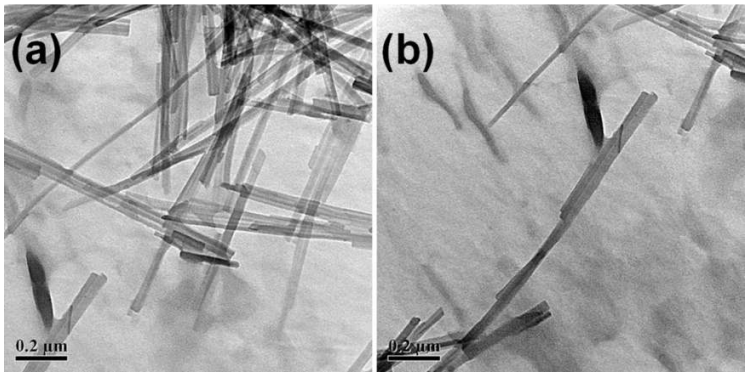

Figure 11: Representative TEM images of (a) C60E40/SP and (b) C60E40/PCL-g-SP nanocomposites

The nanocomposites having homogeneous and uniform filler dispersion with good polymer-filler interfacial adhesion characteristically show synergistic mechanical properties and thermal stability. An effective organic modification of the polar surface of inorganic fillers not only increases filler wettability but also improves the state of filler dispersion. On the contrary, the aggregated microstructure of nanoparticles acts as a point of stress-concentration that leads to deterioration of mechanical properties. The C60E40/SP nanocomposite in Figure 11 (a) contains a large aggregate of sepiolite needles. These aggregates are the clear indication of the poor quality of dispersion of pristine sepiolite in the matrix. Whereas, the C60E40/PCL-g-SP nanocomposite possess a lesser number of aggregates compared to pristine sepiolite based nanocomposite. The representative TEM micrograph of C60E40/PCL-g-SP in Figure 11 (b) clearly shows less sepiolite needle-to-needle contacts. The successful hydrophilization of sepiolite needle by organically modifying with PCL (as evident from the contact angle data) results decrease in the filler-filler interaction. Hence, PCL acts as a compatibilizer between the sepiolite filler and the polymer matrix. The improved state of filler dispersion of the PCL modified sepiolite needles is the outcome of increased polymer-filler interfacial adhesion. However, it is important to mention that breakage of the sepiolite needles in both the nanocomposites during melt processing is inevitable. Hence, the length of sepiolite needles in both the nanocomposites are found to be reduced compared to pristine sepiolite needles. The severe mechanical shear in the highly viscous polymer matrix undoubtedly resulted in fracture of

long and brittle sepiolite needles. The effect PCL modification on the breakage of sepiolite needles is important to understand, and further detail study is necessary to have an insight into it.

Fracture surface morphology using FESEM

The low magnification SEM images in Figure 12 show the overall view of fractured surface morphology of the prepared nanocomposites. The fractured surface of C60E40/PCL-g-SP (Figure 12 (b)) is very rough with a good deal of ridgelines. The presence of such ridgelines indicates the direction of crack propagation along the polymer-filler interface. A closer and magnified view of the ridgelines can be seen from the insets of Figure 12 (b). Such rough surface morphology along with the ridgelines refers good polymer-filler interaction with improved dispersion that may again be related to the improvement in mechanical properties [67].

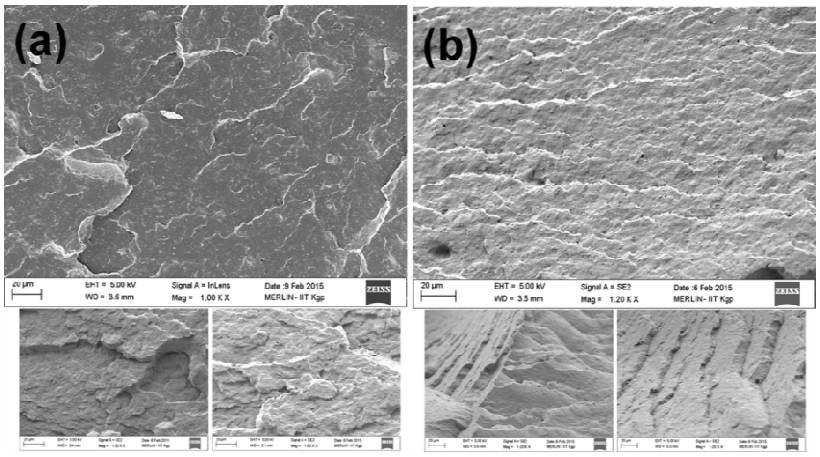

Figure 12: SEM images of cryo-fractured surface of (a) C60E40/SP and (b) C60E40/PCL-g-SP. The corresponding insets show at higher magnifications

On the contrary, the surface of C60E40/SP nanocomposite (Figure 12 (a)) is found to be smooth enough with no crack initiation or propagation. A comparatively smoother fracture surface of the C60E40/SP nanocomposite suggests poor polymer-filler interfacial adhesion that was accompanied by premature, rather brittle type fracture [68]. Such weak interfacial polymer-filler adhesion leads to poor dispersion and inefficient stress transfer that accounts

for inferior mechanical properties [69, 70]. The fracture surface morphology of C60E40/SP at higher magnification is shown in the insets of Figure 12 (a). FESEM images of cryo-fractured samples of pristine and PCL modified SP nanocomposites are illustrated in Figure 13 (a) and (b) respectively in order to unveil the type filler dispersion.

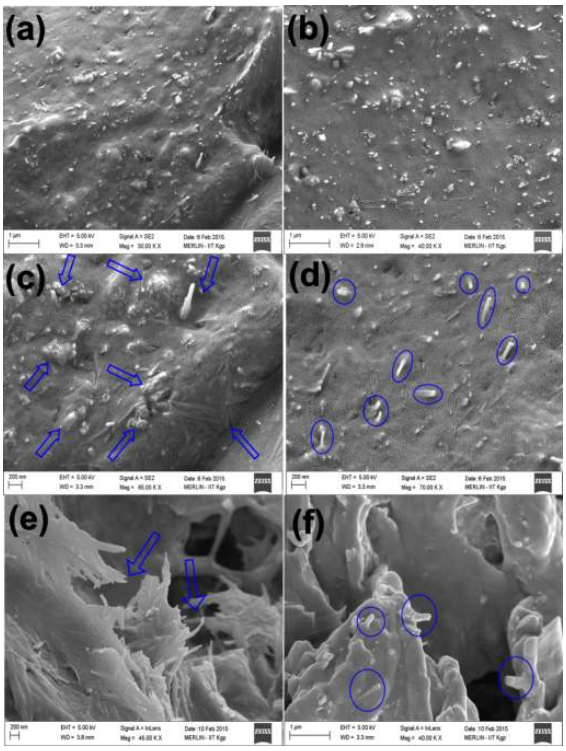

Figure 13: FESEM images of cryo-fractured surface of (a) C60E40/SP and (b) C60E40/PCL-g-SP at low magnification, (c) C60E40/SP and (d) C60E40/PAL-g-SP at high magnification, and tensile fractured image of (e) C60E40/SP and (f) C60E40/PAL-g-SP respectively

A good state of dispersion of nanofiller in the polymer matrix is a prerequisite condition for effective reinforcement. It can be realized that the modified sepiolite needles in Figure 13 (b) are well distributed in the fractured section of C60E40/PCL-g-SP. Interestingly, a very small number of bundles or aggregates of modified sepiolite are observed even at a concentration as high as 5 wt%. Moreover, the filler-polymer interfaces at the filler surface in the magnified image in Figure 13 (d) are vague, which are encircled with blue color. Such an excellent filler distribution in its finest elemental units is a direct implication of

improved polymer-filler adhesion. On the contrary, the pristine sepiolite nanocomposite (C60E40/SP), as shown in Figure 13 (c) contains large number of agglomerates of sepiolite needles (as indicated by arrow marks). The prominent polarity difference between the pristine sepiolite needles and organic polymer matrix increases filler-filler interaction and reduces polymer-filler interaction. Hence, unlike the modified sepiolite, the poor dispersion quality of pristine sepiolite needles in the polymer matrix is because of lack of polymer-filler interface adhesion. An acute manifestation of large agglomerates of pristine sepiolite needles in the polymer matrix can clearly be realized from Figure 13 (c) at high magnification. To find the effect of covalent modification of sepiolite on the micro mechanical failure of nanocomposites, the tensile fracture surfaces are scrutinized using FESEM. The representative photomicrographs of tensile fractured pristine and modified sepiolite needle nanocomposite samples are shown in Figure 13 (e) and (f) respectively. It can be apprehended that the modified sepiolite needles (Figure 13 (f)) are fractured under tensile failure, and no pulled out needles are observed. Here, it is detected that the modified sepiolite needles are well impregnated into the polymer matrix, and the fractured needles are intimately surrounded by the matrix (encircled with blue color). Such morphology of the modified sepiolite needles in C60E40/PCL-g-SP is a clear indication of closer contact between sepiolite needles and polymer matrix, which is because of better wetting of filler by the matrix. On the other hand, extensive pull-out sepiolite needles in large agglomerate are seen in the tensile fractured surface of pristine sepiolite nanocomposite (as indicated by arrow in Figure 13 (e)) that are completely devoid of matrix. This poor morphology implicates an existence of substandard filler wetting in the C60E40/SP nanocomposite.

4. CONCLUSIONS

Hydrophilic pristine sepiolite was covalently modified with poly(ε-caprolactone) (PCL) by following a facile one step ring opening polymerization of ε-caprolactone. An efficient modification of sepiolite was realized from the FTIR, XRD, HRTEM results, and water contact angle measurement. The improved hydrophobicity of PCL modified sepiolite, as indicated by the increased water contact angle value is attributed to the successful and efficient organic modification of sepiolite. Pristine and PCL modified sepiolite based

nanocomposites of chlorinated polyethylene (CPE)/ethylene methacrylate copolymer (EMA) blend were prepared by the conventional melt mixing technique. A notable enhancement (47.77 %) in the tensile strength of C60E40/PCL-g-SP nanocomposite was observed over the neat C60E40 blend. The increased glass transition temperature (T_g) and storage modulus (E') of C60E40/PCL-g-SP from the dynamic mechanical analysis (DMA) well corroborates with the ultimate tensile data. The synergistic mechanical property of C60E40/PCL-g-SP over C6E40/SP and neat C60E40 blend is the result of high polymer-filler interfacial adhesion due to competent grafting of PCL polymer chains onto SP surface (as evident from the HRTEM and water contact angle data). Furthermore, the thermogravimetric analysis (TGA) reveals 38.4% and 39.6% increment in initial degradation temperature (T_i) values of C6E40/SP and C60E40/PCL-g-SP over the neat C60E40 blend. This increase in the T_i value along with higher (%) char yield content of both the nanocomposites compared to the neat blend clearly demonstrates a positive impact of sepiolite needles on thermal degradation stability of C6E40 blend. The morphology study of nanocomposites using XRD, HRTEM, and FE-SEM proposes a better state of sepiolite needle dispersion in C60E40/PCL-g-SP compared to C60E40/SP. Moreover, the micromechanical modeling of "*Pukánszky model*" based on experimental data is in good agreement with morphology results revealing highest interface interaction parameter B value for C60E40/PCL-g-SP. Besides, PCL being compatible with both the polymer provided an added advantage to this (C60E40) blend system in filler dispersion during melt processing. Hence, it can be concluded that in CPE/EMA (60/40) blend system, the one step covalent modification of sepiolite by PCL acts as a feasible method for improving polymer-filler interfacial adhesion that also promotes state of filler dispersion in the nanocomposite.

REFERENCES

1. P. Bhagabati and T. Chaki, *Journal of Applied Polymer Science*, 2014, **131**.
2. D. Paul and L. Robeson, *Polymer*, 2008, **49**, 3187-3204.
3. F. C. Basurto, D. García-López, N. Villarreal-Bastardo, J. C. Merino and J. M. Pastor, *Composites Part B: Engineering*, 2013, **47**, 42-47.

4. N. Moazeni, Z. Mohamad and N. Dehbari, *Journal of Applied Polymer Science*, 2015, **132**, n/a-n/a.
5. M. F. Can, L. Avdan and A. C. Bedeloglu, *Polymer Composites*, 2014, DOI: 10.1002/pc.23147, n/a-n/a.
6. E. Eren and H. Gumus, *Desalination*, 2011, **273**, 276-284.
7. E. G. Huertos, A. Singer and E. Galan, *Developments in Palygorskite-sepiolite Research: A New Outlook on These Nanomaterials*, Elsevier, 2011.
8. A. Sun, J.-B. d'Espinose de la Caillerie and J. J. Fripiat, *Microporous Materials*, 1995, **5**, 135-142.
9. M. Alkan, G. Tekin and H. Namli, *Microporous and Mesoporous Materials*, 2005, **84**, 75-83.
10. A. Corma, H. García, A. Leyva and A. Primo, *Applied Catalysis A: General*, 2004, **257**, 77-83.
11. V. Mittal, *Advances in polyolefin nanocomposites*, CRC Press, 2011.
12. H. Öztürk Düşkünkorur, E. Pollet, V. Phalip, Y. Güvenilir and L. Avérous, *Polymer*, 2014, **55**, 1648-1655.
13. G. Tartaglione, D. Tabuani, G. Camino and M. Moisio, *Composites Science and Technology*, 2008, **68**, 451-460.
14. Y. Zheng and Y. Zheng, *Journal of applied polymer science*, 2006, **99**, 2163-2166.
15. S. Xie, S. Zhang, F. Wang, M. Yang, R. Séguéla and J.-M. Lefebvre, *Composites science and technology*, 2007, **67**, 2334-2341.
16. E. Bilotti, H. Fischer and T. Peijs, *Journal of applied polymer science*, 2008, **107**, 1116-1123.
17. J. Ma, E. Bilotti, T. Peijs and J. Darr, *European Polymer Journal*, 2007, **43**, 4931-4939.
18. D. García-López, J. F. Fernández, J. C. Merino, J. Santarén and J. M. Pastor, *Composites Science and Technology*, 2010, **70**, 1429-1436.
19. F. Zheng, Q. H. Mi, K. Zhang and J. Xu, *Polymer Composites*, 2014, DOI: 10.1002/pc.23150, n/a-n/a.
20. R. E. Grim and R. E. Grim, *Applied clay mineralogy*, McGraw-Hill New York, 1962.
21. C. Fernandez-Barranco, A. Yebra-Rodriguez, M. D. La Rubia-Garcia, F. J. Navas-Martos and P. Alvarez-Lloret, *Polymer Composites*, 2014, DOI: 10.1002/pc.23146, n/a-n/a.
22. E. Duquesne, S. Moins, M. Alexandre and P. Dubois, *Macromolecular Chemistry and Physics*, 2007, **208**, 2542-2550.
23. M. Shafiq, T. Yasin and S. Saeed, *Journal of Applied Polymer Science*, 2012, **123**, 1718-1723.
24. A. Choudhury, A. K. Bhowmick and C. Ong, *Polymer*, 2009, **50**, 201-210.
25. K. Fukushima, D. Tabuani and G. Camino, *Materials Science and Engineering: C*, 2009, **29**, 1433-1441.
26. H. E. Miltner, N. Watzeels, A.-L. Goffin, E. Duquesne, S. Benali, P. Dubois, H. Rahier and B. Van Mele, *Journal of Materials Chemistry*, 2010, **20**, 9531-9542.
27. M. Frydrych, C. Wan, R. Stengler, K. U. O'Kelly and B. Chen, *Journal of Materials Chemistry*, 2011, **21**, 9103-9111.
28. H. L. Zeng, C. Gao and D. Y. Yan, *Advanced Functional Materials*, 2006, **16**, 812-818.
29. K. Rogers, E. Takacs and M. Thompson, *Polymer testing*, 2005, **24**, 423-427.
30. S. Akyüz and T. Akyüz, *Journal of Molecular Structure*, 2003, **651–653**, 205-210.
31. D. M. Moore and R. C. Reynolds, *X-ray Diffraction and the Identification and Analysis of Clay Minerals*, Oxford university press Oxford, 1989.
32. K. Majerska, A. Duda and S. Penczek, *Macromolecular rapid communications*, 2000, **21**, 1327-1332.
33. A. Kowalski, A. Duda and S. Penczek, *Macromolecules*, 2000, **33**, 7359-7370.

34. Ö. Demirbaş, M. Alkan, M. Doğan, Y. Turhan, H. Namli and P. Turan, *Journal of Hazardous Materials*, 2007, **149**, 650-656.
35. C. Wan and B. Chen, *Nanoscale*, 2011, **3**, 693-700.
36. J. Di, L. Jin-quan, Y. Xing-fang and W. Yu-lin, *Journal of Wuhan University of Technology-Mater. Sci. Ed.*, 2004, **19**, 44-47.
37. R. L. Frost, O. B. Locos, H. Ruan and J. T. Kloprogge, *Vibrational Spectroscopy*, 2001, **27**, 1-13.
38. J. Cornejo and M. Hermosin, *Clay Minerals*, 1988, **23**, 391-398.
39. N. M. Ranjha, J. Mudassir and S. Majeed, *Bulletin of Materials Science*, 2011, **34**, 1537-1547.
40. R. Benlikaya, M. Alkan and İ. Kaya, *Polymer Composites*, 2009, **30**, 1585-1594.
41. E. Bilotti, R. Zhang, H. Deng, F. Quero, H. R. Fischer and T. Peijs, *Composites Science and Technology*, 2009, **69**, 2587-2595.
42. L. Bokobza, A. Burr, G. Garnaud, M.-Y. Perrin and S. Pagnotta, *Polymer international*, 2004, **53**, 1060-1065.
43. J.-Z. Liang, *Composites Part B: Engineering*, 2013, **51**, 224-232.
44. B. Pukanszky, *Composites*, 1990, **21**, 255-262.
45. K. Renner, C. Kenyó, J. Móczó and B. Pukánszky, *Composites Part A: Applied Science and Manufacturing*, 2010, **41**, 1653-1661.
46. B. K. Satapathy, M. Ganß, P. Pötschke and R. Weidisch, *Optimization of polymer nanocomposite properties*, 2010, 139-172.
47. M. Selvakumar, S. K. Jaganathan, G. B. Nando and S. Chattopadhyay, *Journal of Biomedical Nanotechnology*, 2015, **11**, 291-305.
48. B. Turcsanyi, B. Pukanszky and F. Tüdõs, *Journal of Materials Science Letters*, 1988, **7**, 160-162.
49. N. Dayma and B. K. Satapathy, *Materials & Design*, 2012, **33**, 510-522.
50. S. Mandal and S. Alam, *Journal of Applied Polymer Science*, 2012, **126**, 724-733.
51. C. Robertson, C. Lin, M. Rackaitis and C. Roland, *Macromolecules*, 2008, **41**, 2727-2731.
52. Rao and J. M. Pochan, *Macromolecules*, 2006, **40**, 290-296.
53. P. B. Messersmith and E. P. Giannelis, *Chemistry of Materials*, 1994, **6**, 1719-1725.
54. L. A. Pothan, Z. Oommen and S. Thomas, *Composites Science and Technology*, 2003, **63**, 283-293.
55. J. W. Gilman, *Applied Clay Science*, 1999, **15**, 31-49.
56. T. D. Hapuarachchi and T. Peijs, *Composites Part A: Applied Science and Manufacturing*, 2010, **41**, 954-963.
57. S. S. Ray and M. Okamoto, *Progress in polymer science*, 2003, **28**, 1539-1641.
58. F. Chivrac, E. Pollet, M. Schmutz and L. Avérous, *Carbohydrate Polymers*, 2010, **80**, 145-153.
59. N. Huang, Z. Chen, C. Yi and J. Wang, *Express Polymer Letters*, 2010, **4**, 227-233.
60. M. Alexandre and P. Dubois, *Materials Science and Engineering: R: Reports*, 2000, **28**, 1-63.
61. H. Chen, M. Zheng, H. Sun and Q. Jia, *Materials Science and Engineering: A*, 2007, **445**, 725-730.
62. N. García, M. Hoyos, J. Guzmán and P. Tiemblo, *Polymer Degradation and Stability*, 2009, **94**, 39-48.
63. A. A. Vassiliou, K. Chrissafis and D. N. Bikiaris, *Thermochimica Acta*, 2010, **500**, 21-29.
64. F.-C. Chiu, S.-W. Fu, W.-T. Chuang and H.-S. Sheu, *Polymer*, 2008, **49**, 1015-1026.

65. N. Jouault, F. Dalmas, F. Boué and J. Jestin, *Polymer*, 2012, **53**, 761-775.
66. B. Lepoittevin, M. Devalckenaere, N. Pantoustier, M. Alexandre, D. Kubies, C. Calberg, R. Jérôme and P. Dubois, *Polymer*, 2002, **43**, 4017-4023.
67. A. Das, F. R. Costa, U. Wagenknecht and G. Heinrich, *European Polymer Journal*, 2008, **44**, 3456-3465.
68. P. L. Teh, Z. A. Mohd Ishak, A. S. Hashim, J. Karger-Kocsis and U. S. Ishiaku, *European Polymer Journal*, 2004, **40**, 2513-2521.
69. N. Dayma and B. K. Satapathy, *Materials & Design*, 2010, **31**, 4693-4703.
70. M. Kotal, S. K. Srivastava and A. K. Bhowmick, *Polymer International*, 2010, **59**, 2-10.